An Efficient FWGN-Based Modelling And Simulation Scheme For The Suzuki Flat Fading Channel

Michel Mfeze[1], Emmanuel Tonye[2]

[1,2]Department of Electrical and Telecommunications Engineering, National Advanced School of Engineering, University of Yaoundé I, Cameroon,
Corresponding Author: Michel Mfeze

Abstract: *This paper optimizes the FWGN-based Suzuki fading stochastic model for the frequency-nonselective land mobile radio channel as this composite Rayleigh-Lognormal distribution represents the worst-case fading. In a previous work, the Young & Beaulieu simulator was identified to be a better Rayleigh channel model. The lognormal fading generator is then optimized through the study of various digital filters allowing the choice of the best compromise considering the environment, required fading statistics and shadowing severity level. Both Finite and Infinite Impulse Response filters are evaluated. Filters discrimination criteria are the magnitude and phase responses, the minimum required order and thus hardware implementation cost, the shadowing outage probability and autocorrelation, as well as the statistical divergence between the simulated and theoretical shadowing distributions in LTE environments. The Bhattacharyya distance is therefore computed using a Monte Carlo method. The proposed Suzuki fading simulator, its output signal and various order statistics are finally presented.*

Keywords: *Rayleigh fading, shadowing, lognormal fading, Suzuki fading, channel modelling, FWGN, IIR filter, FIR filter, statistical distance, autocorrelation, outage probability, LTE*

I.   Introduction

The frequency-nonselective land mobile radio channels are characterized by two types of fading effects: large-scale fading and small scale fading. Large-scale fading is the slow variation of the mean distant-dependent signal power over time. This depends on the presence of obstacles in the signal path and on the position of the mobile unit. Small-scale fading is also called multipath fading because if a large number of reflective paths is encountered, the received signal envelope is the combination of many replicas of the original signal arriving at receiver from many different paths. The signal on these different paths can constructively or destructively interfere with each other **[1]**. The simplest stochastic model processes to be applied to this are Rayleigh and Rice processes. However, the flexibility of these models is too limited and often not large enough for a sufficient adaptation to the statistics of real-world channels. For the frequency-nonselective land mobile radio channel, the Suzuki process appears to be a more suitable and adequate stochastic model **[2]**.

Hirofumi Suzuki **[3]** introduced the Suzuki distribution in 1977 to characterize the urban radio propagation channel in various urban environments. Suzuki fading combines small scale or fast fading from multipath and large scale or slow/long-term fading due to shadowing from reflection and diffraction. The large scale follows a lognormal distribution and the small scale follows a Rayleigh distribution. The lognormal process takes into account the slow time variation of the average local received power, whereas the Rayleigh process models the fast fading. The composite Rayleigh-Lognormal distribution represents a worst-case scenario, which is frequently used in macrocells as a benchmark for system performance, and base stations deployment studies as it assumes that a direct line-of-sight component is absent due to shadowing **[4]**. Usually, it is also assumed that the Gaussian random processes, which produce the Rayleigh process, are uncorrelated **[2].**

Lognormal amplitude fluctuations arise from the motion of the receiver in different environments such as urban areas, flat-open terrain, hilly terrain, etc. The parameters relevant for lognormal fading are the speed, the local constant, and standard deviation. Generally, the higher the speed of the receiver is, the faster the variations in signal amplitude are. The local constant is a measure for the distance over which fading conditions do not change. In strongly structured areas, the local constant will have low values, for example tens of meters in street canyons, whereas on wide plains with little vegetation high values even greater than hundreds of meters, can be expected **[2].** The higher the lognormal constant is, the slower the variations in signal amplitude are.

Many previous works have focused on the Suzuki channel modeling, proposing deterministic models based on the sum of sinusoids method and stochastic models based on the filtered white Gaussian noise (FWGN) method **[2][3][4][5][6].** The classical and a generalized Suzuki process was presented in Suzuki, 1977 **[3]**. By

---

assuming the Gaussian noise sources for the Rayleigh fading generator being correlated, Krantzik et al, 1990 **[6]** proposed the so-called modified Suzuki process. In Pätzold, 1990 **[2]**, an extended Suzuki process of type I, where the Rayleigh process is substituted by a Rice process taking the influence of a line-of-sight component into account is presented as well as the extended Suzuki process of Type II, which is a product process of the extended Rice process and the lognormal process. This was to make the model more suitable for the satellite mobile radio channels.

The simulator in Wirastuti et al, 2008 **[5]** generates correlated Rayleigh and lognormal random variables using fourth order Butterworth low pass filters. The stochastic simulators proposed in Pätzold, 1990 **[2]** are based on low pass filters with an additional Hilbert transformer on the quadrature component for the Rice process generator, and for the lognormal process, a real valued low pass filter whose transfer function $H(f)$ is related to the Gaussian power spectral density $S_g(f)$ by $H(f) = \sqrt{S_g(f)}$.

In most cases, the low pass filter for the fading process is chosen on a single criteria basis like amplitude response or hardware complexity. In the present work a Suzuki fading generator for cellular land mobile radio channels is proposed using the FWGN method. The findings in Mfeze et al, 2015 **[7]** are considered for the choice of an efficient FWGN-based Rayleigh simulator whereas the lognormal fading generator is optimized through the study of various digital low pass filters allowing the choice of the best option according to the environment, required fading higher order statistics and the desired fading severity or shadowing level. We considered both Finite Impulse Response (FIR) and Infinite Impulse Response (IIR) filters. Although FIR are always stable and adequate for fixed point implementation, their delay is often much greater than for equal performances IIR filter **[8].**

Filters discrimination hereby takes into consideration the magnitude and phase responses, minimum required filter order and thus filter realization hardware complexity, divergence or statistical distance between the simulated and theoretical shadowing distributions in a LTE environment as well as various orders statistics of the resulting signals.

II. The Suzuki Fading Generation Process
2.1. Probability Distributions Involved in the Suzuki Fading
2.1.1. The Lognormal Distribution

A random variable ψ is said to have the lognormal distribution with parameters $\mu \in \mathbb{R}$ and $\xi > 0$ if $\ln(\psi)$ has the normal distribution with mean μ and standard deviation ξ. The probability density function (PDF) of the lognormal distribution is given by

$$p_{log}(\psi) = \begin{cases} \frac{1}{\psi\xi\sqrt{2\pi}} e^{-\frac{(ln\psi - \mu)^2}{2\xi^2}} & \psi \geq 0 \\ 0 & \psi < 0 \end{cases} \tag{1}$$

With $\mu = \overline{ln\,\psi}$ and $\xi^2 = \overline{(ln\,\psi - \mu)^2}$. Where μ and ξ are the mean and standard deviation of $ln\,\psi$. In decibel units we have

$$p_{log}(r) = \begin{cases} \frac{\beta}{\psi\xi_{dB}\sqrt{2\pi}} e^{-\frac{(10log_{10}(\psi) - \mu_{dB})^2}{2\xi_{dB}^2}} & \psi \geq 0 \\ 0 & \psi < 0 \end{cases} \tag{2}$$

With $\beta = 10/ln10$. The standard deviation is a measure for the power deviation of the amplitude fluctuations, i.e. it is a measure for how strongly the amplitude varies in power over time. The higher the standard deviation is, the larger the variations in signal amplitude are. The mean and standard deviations are determined from large scale propagation model in the environment of interest. The expected value and the variance of lognormally distributed random variables η are given by **[2]**

$$E\{\eta\} = \psi\sqrt{\frac{\pi}{2}}e^{\mu+\frac{\xi^2}{2}} \tag{3}$$

$$Var\{\eta\} = \left(2e^{\xi^2} - \frac{\pi}{2}\right).\psi^2 e^{2\mu+\xi^2} \tag{4}$$

The cumulative distribution functions (CDF) is:

$$F_{log}(\psi) = \frac{1}{\xi\sqrt{2\pi}}\int_{-\infty}^{\psi}\frac{1}{t}e^{-\frac{(\ln t - \mu)^2}{2\xi^2}}\,dt = \frac{1}{2} + \frac{1}{2}erf\left(\frac{\ln\psi - \mu}{\xi\sqrt{2}}\right) \tag{5}$$

2.1.2. The Rayleigh Distribution

The PDF of the Rayleigh distribution is given by

$$p_{ray}(r) = \begin{cases} \frac{r}{\sigma^2}e^{-\frac{r^2}{2\sigma^2}} & r \geq 0 \\ 0 & r < 0 \end{cases} \tag{6}$$

The CDF for the envelope is given by

$$F_{ray}(r) = \int_0^r \frac{t}{\sigma^2}e^{-\frac{t^2}{2\sigma^2}}\,dt = 1 - e^{-\frac{r^2}{2\sigma^2}} \tag{7}$$

The mean and the variance of the Rayleigh distribution are $\sigma\sqrt{\pi/2}$ and $(2-\pi/2)\sigma^2$, respectively.

2.1.3. The Suzuki Distribution

The fading concerns only multipath component which is Rayleigh distributed but its average power, described by parameter $2\sigma^2$ varies with lognormal distribution for longer sections of series. Its PDF can be written as:

$$p_{suz}(r) = p_{ray}(r).p_{log}(r) \tag{8}$$

Or

$$p_{suz}(r) = \begin{cases} \int_0^{\infty}\frac{1}{\xi\sigma\sqrt{2\pi}}e^{-\frac{(\ln\sigma - \mu)^2}{2\xi^2}}\cdot\frac{r}{\sigma^2}e^{-\frac{r^2}{2\sigma^2}}\,d\sigma & r \geq 0 \\ 0 & r < 0 \end{cases} \tag{9}$$

Where σ is the mode or the most probable value of the Rayleigh distribution, ξ is the shape parameter of the lognormal distribution. However, a practical limitation to this distribution is that no closed form has been found to solve the CDF integral **[3].**

2.2. Suzuki Fading Generation by the FWGN Method
2.2.1. Generating Rayleigh Fading by the FWGN Method

In-phase I and quadrature Q components concept are used to simulate Clark and Gans fading model as shown in Figure 1. The filtered white Gaussian noise method for the fading sequence generation is also used.
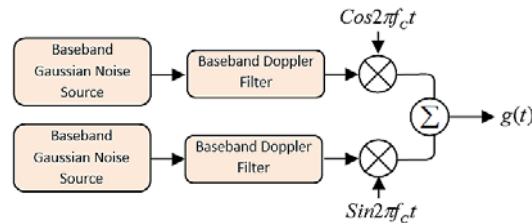

Figure 1. Clarke and Gans model

Let $H(f)$ be the frequency response of a filter and $x(t)$ a signal with power spectral density $p_x(f)$ being filtered. The power spectral density $p_y(f)$ of the output signal $y(t)$ is given by:
$$p_y(f) = p_x(f)|H(f)|^2 \tag{10}$$

In order to generate In- phase and quadrature components of the channel complex coefficients, each having a Doppler spectrum $p_y(f) = S(f)$, one needs to filter white Gaussian noise with power spectral density $N_0/2$ through a filter $H(f)$ with frequency response

$$H(f) = \sqrt{\frac{2}{N_0} S(f)}$$ (11)

Which can be implemented either by Inverse Discrete Fourier Transform (IDFT) or by a regressive filter. This filter is more likely a shaping filter as it determines the power spectrum shape and the temporal correlation function of the fading process.

2.2.2. The Young and Beaulieu Simulator to Generate the Rayleigh Fading

Young's model among FWGN models, appeared to be a better channel modelling and simulation tradeoff for frequency nonselective Rayleigh fading channel [7]. Evaluation metrics like temporal complexity, bit error rate (BER), and second order statistics like autocorrelation, level crossing rate (LCR) and average fade duration (AFD) were used. The simulated parameters for this model appeared to be the best agreement with theoretical curves with a better correlation for delays less than 10ms.

From the Clarke and Gans model, David J. Young and Norman C Beaulieu derived a model based on IDFT which is a kind of a modified Clarke and Gans model [9]. According to the authors, this model uses half of the IDFT and only 2/3 of spatial complexity compared to Smith's model. Extensive simulations showed that a similar performance is obtained for temporal complexity (Young's model temporal complexity≈ 70% of Smith's model temporal complexity) [7].

Two independent identically distributed (i.i.d) random Gaussian processes of N components with zero mean and unit variance are generated and filtered by two identical low-pass Doppler filter of frequency response $\{F[k]\}$ in order to get correlated signals. The two In-Phase and Quadrature components are added and the result is passed through a IFFT module which gives the channel output signal. The white Gaussian noise processes are imposed to be uncorrelated to comply with the WSSUS (Wide Sense Stationary and Uncorrelated Scattering) assumption.

Figure 2 shows the Rayleigh component generated by the Young fading simulator.
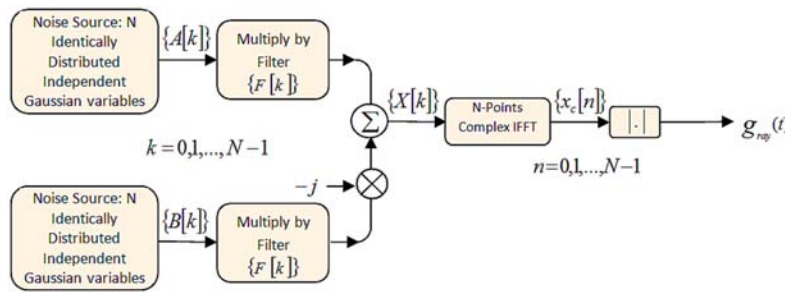

Figure 2. Young's Fading simulator

The Young's Doppler filter is defined below:

$$F_m(k) = \begin{cases} 0, & k = 0 \\ \sqrt{\dfrac{1}{2\sqrt{1-\left(\frac{k}{Nf_m}\right)^2}}}, & k = 1,2,\ldots,k_m - 1 \\ \sqrt{\dfrac{k_m}{2}\left[\dfrac{\pi}{2} - arctan\left(\dfrac{k_m-1}{\sqrt{2k_m-1}}\right)\right]}, & k = k_m \\ 0, & k = k_m + 1,\ldots,N - k_m - 1 \\ \sqrt{\dfrac{k_m}{2}\left[\dfrac{\pi}{2} - arctan\left(\dfrac{k_m-1}{\sqrt{2k_m-1}}\right)\right]}, & k = N - k_m \\ \sqrt{\dfrac{1}{2\sqrt{1-\left(\frac{N-k}{Nf_m}\right)^2}}}, & k = N - k_m + 1,\ldots,N - 1 \end{cases}$$ (12)

With $f_m = \frac{f_{Dmax}}{f_s}$ and $k_m = \lfloor N f_m \rfloor$.

Where $\lfloor x \rfloor$ represents the maximum integer less than or equal to x. The length of the Rayleigh fading sequence generated by this simulator depends on the length of the noise sources which must be high enough to get a reasonable fading sequence length.

2.2.3. Generating the Lognormal Fading by the FWGN Method

Lognormal processes $g_{log}(t)$ can be derived by means of the nonlinear transform.

$$g_{log}(t) = 10^{(\xi\gamma(t)+\mu)/20} \tag{13}$$

$\gamma(t)$ is a real-valued Gaussian random process with expected value zero and unity variance. The generation of correlated lognormal random variable uses a filter. N samples of the independently distributed white Gaussian noise $\eta(t) \sim N(0; 1)$ are generated and filtered with a real-valued low-pass filter, with transfer function $H(f)$. The result is a correlated Gaussian random variable. $H(f)$ can be related to the power spectral density $S(f)$ of the process $\eta(t)$ by $H(f) = \sqrt{S(f)}$. The Gaussian power spectral density is assumed in the form [2].

$$S(f) = \frac{1}{\sigma_c\sqrt{2\pi}} e^{-\frac{f^2}{2\sigma_c^2}} \tag{14}$$

where the 3dBcut-off frequency $f_{co} = \sigma_c\sqrt{2ln2} = f_{Dmax}\sqrt{ln2}$ is in general much smaller than the maximum Doppler frequency f_{Dmax}. Other types of power spectral densities $S(f)$ than the above form can be found in literature [7].

As an alternative, FIR and IIR lowpass filters (LPF) of a specific order can be applied and choosing an efficient filter for this option is explored in this paper. In this case, for a given Doppler frequency f_{Dmax}, the cut-off frequency f_{co} is normalized by the Nyquist frequency, $f_{con} = f_{co}/f_{nyq}$ given f_{nyq} wich is at least twice the Doppler frequency(Doppler bandwidth) and is half of the sampling frequency. Also, implementing a digital system with a bandwidth B will require a sampling rate of at least 2B according to the Nyquist sampling theorem. Generally, the sampling rate is chosen to control aliasing to tolerable levels. According to Jeruchim et al, 2000 [10], 8–16 samples/Hz is adequate but we will be using a wider range including the minimum required 4 samples/Hz. Therefore, the Nyquist frequency f_{nyq}, the Doppler frequency f_{Dmax} and the sampling rate f will be related as follows.

$$4. f_{Dmax} \le f_s = 2f_{nyq} \le 16. f_{Dmax} \tag{15}$$

The correlated Gaussian random variable at the LPF output is then scaled by $\rho = \xi/\Omega$ where ξ is the standard deviation of the normal process and Ω is the overall gain of the filter given by [11]:

$$\Omega = \int_{-\infty}^{+\infty} |H(f)| df \tag{16}$$

The result is added to μ which practically represents the mean shadow level. Finally, applying an antilogarithmic operation gives the correlated lognormal random variable as shown on Figure 3.
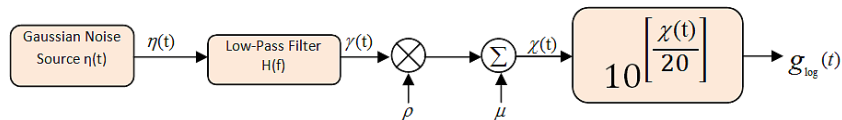

Figure 3. Lognormal shadowing simulator

III.   IIR And FIR Filters For Shadowing

3.1. The Infinite Impulse Response Filter

The filter output y(m) is computed as a weighted, finite term sum, of past, present, and perhaps future values of both the filter input x(m) ant output. The filter includes both feedback and feed forward terms. The general IIR difference equation is given by

$$y(m) = \sum_{l=1}^{p} a_l y(m-l) + \sum_{k=0}^{n} b_k x(m-k) \tag{17}$$

Various IIR lowpass filters like Butterworth, Chebyshev, Inverse Chebyshev and Cauer filters are investigated in this paper.

3.1.1. The Butterworth Low-Pass Filter

The magnitude of the frequency response of this family of filters can be written as

$$|H_{Butt}(f)| = \sqrt{\frac{H_0}{1 + \left(\frac{f}{f_{co}}\right)^{2n}}} \tag{18}$$

Where f_{co} represents the bandwidth or the 3dB cut-off frequency and n the order of the filter. H_0 is the DC gain or gain at zero frequency and can be normalized to 1 [12]. The attenuation is -3dB at the cutoff frequency and -20dB above. The pass band ripple δ_1 or maximum pass-band attenuation factor is given in dB by

$$\delta_{1dB} = 10 log_{10}(1 + \varepsilon^2) \tag{19}$$

since

$$\delta_1 = \frac{1}{\sqrt{1 + \varepsilon^2}} \tag{20}$$

Given the minimum stop-band attenuation factor δ_2, the pass-band edge f_{co} and the stop-band edge f_{sb}, the filter order is defined by

$$n = \left| \frac{log\left(\frac{\varepsilon}{\sqrt{\delta_2^2 - 1}}\right)}{log\left(\frac{f_{co}}{f_{sb}}\right)} \right| + 1 \tag{21}$$

Practically f_{co} and f_{sb} are normalized by the Nyquist frequency. Let f_{con}, f_{sbn} be the normalized frequencies respectively. The filter can then be precisely designed by the knowledge of the four parameters $f_{con}, f_{sbn}, \delta_1$ and δ_2.

3.1.2. The Chebyshev Low-Pass Filter

This filter gets its name because the Chebyshev filter minimizes the height of the maximum ripple, which is the Chebyshev criterion and its mathematical characteristics are derived from Chebyshev polynomials. The magnitude of the frequency response of this family of filters can be written as

$$|H_{Cheb}(f)| = \sqrt{\frac{1}{1 + \varepsilon^2 T_n^2\left(\frac{f}{f_{co}}\right)}} \tag{22}$$

Where ε the ripple factor is described by equation (19), f_{co} is the cutoff frequency and T_n is a first kind Chebyshev polynomial of the nth order.

$$T_n(x) = \begin{cases} cos(n \cos^{-1} x) & |x| \le 1 \\ cosh(n \cosh^{-1} x) & |x| > 1 \end{cases} \tag{23}$$

The cutoff frequency at -3 dB is not applied to Chebyshev filters. It is taken as the point at which the gain falls to the value of the ripple for the final time and has the value δ_1 previously defined.

The passband ripple is given in dB by equation (19). As this parameter is an undesirable one, a value of 1dB or less would be acceptable. The filter order n is then given by [13].

$$n = \left| \frac{\cosh^{-1}\left(\frac{\sqrt{1-\delta_2{}^2}}{\varepsilon\delta_2}\right)}{\cosh^{-1}\left(\frac{f_{sb}}{f_{co}}\right)} \right| + 1 \tag{24}$$

3.1.3. The Inverse Chebyshev Low-Pass Filter

Its magnitude response is given by

$$|H_{InvCheb}(f)| = \sqrt{\frac{T_n{}^2\left(\frac{f_{sb}}{f}\right)}{T_n{}^2\left(\frac{f_{sb}}{f}\right)+\varepsilon^2 T_n{}^2\left(\frac{f_{sb}}{f_{co}}\right)}} \tag{25}$$

The transfer function shows both poles and zeros. The design of such a filter also requires the knowledge of parameters like the maximum pass-band attenuation factor δ_1, and the minimum stop-band attenuation factor δ_2 previously defined. The above parameters allow the computation of the ripple factor ε, the filter order n and the poles and zeros of the transfer function. The minimum stop-band attenuation factor δ_2 also known as the stopband ripple peak value is defined as:

$$\delta_2 = \frac{1}{\sqrt{1+\varepsilon^2 T_n{}^2\left(\frac{f_{sb}}{f_{co}}\right)}} \tag{26}$$

The filter order n is then given by

$$n = \left| \frac{\cosh^{-1}\left(\frac{\sqrt{1-\delta_2{}^2}}{\varepsilon\delta_2}\right)}{\cosh^{-1}\left(\frac{f_{sb}}{f_{co}}\right)} \right| + 1 \tag{27}$$

3.1.4. The Elliptic Low-Pass Filter
Also known as Cauer filters, elliptic filters are equiripple in both the passband and stopband. The amount of ripple in each band is independently adjustable. Its magnitude response is given by

$$|H_{Cauer}(f)| = \frac{1}{\sqrt{1+\varepsilon^2 R_n{}^2\left(k,\frac{f}{f_{co}}\right)}} \tag{28}$$

k is the selectivity factor.

$$0 \le k = \frac{f_{co}}{f_{sb}} < 1 \tag{29}$$

R_n is the n_{th}-order elliptic rational function defined as follows.

$$R_n(k,x) = \begin{cases} r_1 x \prod_{r=1}^{\frac{n-1}{2}} \frac{x^2 - sn^2\left(\frac{2r}{n}K;k\right)}{x^2 - \left[ksn\left(\frac{2r}{n}K;k\right)\right]^{-2}} & for\ n\ odd \\ r_2 \prod_{r=1}^{\frac{n}{2}} \frac{x^2 - sn^2\left(\frac{2r-1}{n}K;k\right)}{x^2 - \left[ksn\left(\frac{2r-1}{n}K;k\right)\right]^{-2}} & for\ n\ even \end{cases} \tag{30}$$

With $x = cd\left(\omega K\left(\frac{1}{k}\right),\frac{1}{k}\right)$

K is the complete elliptic integral, sn is the Jacobi elliptic sine and cd is one of the 12 Jacobi functions **[14] [15].**

$$K(k) = \int_0^{\pi/2} \frac{d\theta}{\sqrt{1-k^2 sin^2\theta}} \tag{31}$$

$$cd(z,k) = \sqrt{\frac{1-sn^2(z,k)}{1-k^2sn^2(z,k)}} \tag{32}$$

The selectivity factor k is also the modulus of the elliptic integral. The parameters r_1 and r_2 are normalizing constants chosen so that $R_n(k,1) = 1$. The value of the ripple factor specifies the passband ripple, while the combination of the ripple factor and the selectivity factor specify the stopband ripple. The filter order n is then given by [16]

$$n = \left\lfloor \frac{K\left(\frac{1}{k}\right)}{K\left(\sqrt{1-\frac{1}{k}}\right)} \right\rfloor + 1 \tag{33}$$

3.2. The Finite Impulse Response Filter

The filter output y(m) is computed as a weighted, finite term sum, of past, present, and perhaps future values of the filter input x(m).

$$y(m) = \sum_{k=0}^{n} b_k x(m-k) \tag{34}$$

If the filter is a direct form filter, b_k is also a filter coefficient. The impulse response or the output in response to a Kronecker delta input, of an nth-order discrete-time FIR filter lasts exactly $n + 1$ samples (from first nonzero element through last nonzero element) before it then settles to zero.

$$h(m) = \sum_{k=0}^{n} b_k \delta(m-k) \tag{35}$$

The frequency response is given by

$$|H_{FIR}(\omega)| = \sum_{k=0}^{n} h(k)e^{-j\omega k} \tag{36}$$

Here $\omega = 2\pi f/f_s$ represents frequency in normalized units (radian/sample). $h(k)$ is the value of the impulse response at the instant k, $0 \le k \le n$ for a FIR filter of order n.
The filter order n is then approximated by

$$n \approx \frac{2}{3} log_{10} \left\lfloor \frac{1}{10\delta_1\delta_2} \right\rfloor \frac{f_s}{f_{sb}-f_{co}} + 1 \tag{37}$$

With δ_1 and δ_2 in natural units. The FIR filter requires no feedback, is inherently stable and present a linear phase. Many filter design methods are available in literature like the Window design method, the Frequency Sampling method, the Weighted least squares design method, the Parks-McClellan method (also known as the Equiripple, Optimal, or Minimax method), and the Equiripple FIR filters that can be designed using the FFT algorithms. In this paper, we are interested in the Parks-McClellan method which allows the design of a constrained optimal order and equiripple FIR filter [17].

IV.   Shadowing Characterization
4.1. Divergence from the Theoretical Lognormal PDF: The Bhattacharyya Distance

Various distance measures exist that are applicable to compare two probability density functions. Computing the distance/divergence between two PDFs P and Q can be regarded as the same as computing the Bayes (or minimum misclassification) probability. This is equivalent to measuring the overlap between two PDFs as the distance. We chose the Bhattacharyya distance which provides bounds on the Bayes misclassification probability. It is expressed as follows

$$d_B(P,Q) = -\ln(\Lambda(P,Q)) = -\ln\left(\int \left(\frac{dP}{d\vartheta},\frac{dQ}{d\vartheta}\right)^{1/2}\right)d\vartheta \tag{38}$$

For discrete probability distributions, we have

$$d_B(P,Q) = -ln \sum_{i=1}^{n} \sqrt{P_i Q_i} \tag{39}$$

Where n is the number of partitions in P and Q. $dP/d\vartheta$ is the Radon-Nykodym derivative of P with respect to ϑ. Λ is the Bhattacharyya coefficient which can be used to determine the relative closeness of the two samples being considered. $\Lambda = 1$ or $d_B(P,Q) = 0$ if P=Q and $\Lambda = 0$ or $d_B(P,Q) = +\infty$ if P is orthogonal to P.

Numerous other discrete distances or divergences are available in literature of probability and information theory like the Earth-Mover's distance (EMD), the Cosine distance, the Kullback-Leibler divergence, the Chi Square distance, the Chebyshev distance, the Hamming distance, the Hellinger distance, the Jensen–Shannon divergence or the City block distance. They will be used in the background to confirm the result given by the Bhattacharyya distance but will not be defined. For more reading about those statistical distances, please refer to Sung-Hyuk, 2007 [18].

4.2. The Severity of Shadowing

The severity of the shadowing is expressed in terms of the standard deviation of the shadowing. The relationship between mean and standard deviation in natural units and in dB [19] is given by:

$$\mu_{db} = \frac{10}{ln10} \mu \tag{40}$$

$$\xi_{db} = \frac{10}{ln10} \xi \tag{41}$$

$\xi = 0dB$ means no shadowing or no slow fading. The standard deviation for lognormal shadowing can vary from 1 to 12dB depending on the environment. This range is commonly used for most communication systems operating over lognormal fading channels [20]. The mean value can be taken as the expected median signal level found using the path loss predicted by the propagation model. Three levels of severity can be defined: Light, Moderate and Heavy shadowing. [21]. A value of 8dB is typically used in LTE CDMA and WIMAX link budget. Also, many authors defined approximate or expected values of the lognormal standard deviation according to various environments. [10][19][21][23][24][25][26][27][28] This has been synthesized in Table 1.

Table 1. Lognormal shadowing standard deviations

Environment (SCM, 3GPP, LTE)	ξ (dB)	Typical ξ (dB)	Severity
Rural	$0 \leq \xi < 6$	3	Light
Forested Rural	$6 \leq \xi \leq 8$	6	Moderate
Suburban	$6 \leq \xi \leq 8$	6	Moderate
Common Urban/ SubUrbanMacrocell	$5 \leq \xi \leq 9$	8	Moderate
Dense Urban/ Urban Microcell/Vehicular Macrocell/ Pedestrian Microcell/ Outdoor to Indoor Microcell NLOS	$8 < \xi \leq 13$	10	Heavy
Indoor	$10 \leq \xi$	12	Heavy

4.3. The Shadowing Autocorrelation

The shadow fading is spatially correlated and its value changes slowly with the movement $\Delta x = v.\Delta t$ of the transmitter or the mobile unit. The autocorrelation coefficient of shadowing is given by the Gudmundson model which is a first-order autoregressive process and follows an exponential decay [23][29][30].

$$R_{xx}\{F(x)F(x + \Delta x)\} = \xi_{db}^2 e^{-\frac{|\Delta x|}{x_c}} = \xi_{db}^2 e^{-\frac{v|\Delta t|}{x_c}} \tag{42}$$

F is the shadowing power and x_c is the equivalent decorrelation distance also known as the shadowing-based equivalent stationarity distance. This is the distance at which the signal autocorrelation equals 1/e of its maximum value. It is on the order of 5 to 50m depending on the environment typically 20m for urban areas and about 5m in rural areas.

For convenience, the simple path loss model derived from the FRIIS model can be used for general tradeoff analysis. For a receiver at distance d from the eNodeB, the received power P_r is related to the transmitted power P_t as follows:

$$P_r = P_t K \left(\frac{d_0}{d}\right)^{\Gamma} = P_t G_t G_r \left(\frac{\lambda}{4\pi d_0}\right)^2 \left(\frac{d}{d_0}\right)^{\Gamma} = P_{r0} \left(\frac{d}{d_0}\right)^{\Gamma} \tag{43}$$

Where d_0 is the close-in reference distance, Γ is the path loss exponent, G_t and G_r are the transmit and receive antenna gains, and λ is the wavelength. Finally, considering the slow fading component X_0, the dB attenuation model is given by:

$$P_{r\,dBm} = P_{r0\,dBm} - 10\Gamma log_{10}\left(\frac{d_0}{d}\right) + X_{0\,dB} \tag{44}$$

4.4. The Outage Probability

The outage probability is a measure of the quality of the transmission in a mobile radio channel. Outage occurs when the SINR at the input of the receiver chain is falling below a certain threshold level. Estimation of outage probability requires knowledge of PDF of sum of lognormal random variables representing the shadowing so determining CDF of sum of correlated lognormal RVs is a pre-requisite. An analytical expression of the outage probability in a lognormal fading scenario based on the fluid model is proposed in **[31].**

$$P_r\{SINR_i(h,v) < \gamma_i\} = Q\left(\frac{10log_{10}(\frac{1}{\gamma_i})-\mu_f}{\xi_f}\right) \tag{45}$$

With

$$Q(x) \triangleq p(Z > x) = \frac{1}{\sqrt{2\pi}}\int_x^{+\infty} e^{-\frac{t^2}{2}}\,dt = \frac{1}{2}erfc(\frac{x}{\sqrt{2}}) \tag{46}$$

Q is the complementary standard Gaussian distribution. γ_i is the power threshold for user i. *SINR* is the Signal to Noise plus Interference Ratio in logarithmic units and h is the channel gain. v is the activity factor of the source. The parameters μ_f and ξ_f are the mean and standard deviation of the shadowing in the presence of multiple co-channel interferers. They could be computed through moment matching approximations using Wilkinson's approach for light shadowing ($\xi_f < 4dB$) and Schwartz & Yeh's approach for moderate and severe shadowing.**[32][33]**.These approaches assume the sum of lognormal random variables is also a lognormal random variable.

V.   Methodology

The Suzuki fading channel model considers both fast fading and slow fading and can be generated by multiplying a Rayleigh fading channel with the lognormal channel. The findings in **[7]** were used for the choice of an efficient Rayleigh fading simulator. For the lognormal channel simulator, the optimization is performed on the low pass filter used to generate correlated Gaussian samples, according to the environment, required fading higher order statistics and the desired fading severity or shadowing level. Both IIR and FIR filters are considered. Filters discrimination takes into consideration the magnitude and phase responses, minimum required filter order and thus filter realization hardware complexity, divergence between the simulated and theoretical shadowing distributions in a typical LTE environment through a statistical distance (Bhattacharyya), and high order statistics like autocorrelation and shadowing outage probability.

The performances of the filters are first compared in term of magnitude or frequency response. We then consider filter parameters commonly used in communication systems to compute minimum required filters order. That is less than 1dB of ripple in the passband defined from 0 to f_{co} and at least 60 dB of minimum stop-band attenuation. A normalized transition width of 0.3 is also considered. Minimizing the hardware implementation cost of filters is an important criterion. This depends on the filter length and is evaluated in terms of required number of filter coefficients, states, adders and multipliers.

Furthermore, assuming an initial N samples of the independently distributed white Gaussian noise $\eta(t) \sim N(0; 1)$ which are uncorrelated. In order to get correlated lognormal random variable, we use a low-pass filter. But we wish to keep the simulated shadowing statistically as close as possible to the known theoretical shadowing distribution. That is to minimize the distance between both distributions. This is achieved using a statistical divergence metric that apply to histograms which is the Bhattacharyya distance. The distance is computed using a Monte Carlo method and averaging the results for thousands of iterations.

Second order statistics of the resulting shadowing like autocorrelation and outage probability are also evaluated with comparison plots presented. For the outage probability, the effect of co-channel interferers is neglected for simplicity. Also, we considered a path loss exponent of 3 for urban and sub urban, a reference distance of 1m, the same antenna gain of 1dB on both the transmitter and receiver and a transmitter power of 1mW

Finally the proposed Suzuki simulator is presented as well as its performance and some of its various order statistics.

VI.   Results And Discussion
6.1. Low-Pass Filters Discrimination
6.1.1. The Filter Minimum Required Order

Here we are looking for a normalized cut-off frequency varying from 1/8 to 1/2 and we need to design a lowpass filter with less than 1dB of ripple in the passband defined from 0 to f_{co} and at least 60 dB attenuation in the stopband. The width of the transition band is set to 0.3 the Nyquist frequency.

Hence $1/8 \leq f_{con} \leq 1/2 < f_{sbn}$, $f_{sbn} = f_{con} + 0.3$, $\delta_1 = 1$ and $\delta_2 = 60$. The computed minimum filter order for all the filter types is given in Table 2. The low-pass filter cut-off frequency should be close or ideally equal to the Doppler frequency **[26]**.

The table shows the Caeur (elliptic) filter for any set of design data meets filter requirements with the lowest minimum filter order. The Chebyshev filters have similar order while the Butterworth filter shows the highest minimum order among all IIR filters. The table also shows the Direct-form FIR filter meets filter requirements with a much more higher minimum order, and three times the best IIR case.

Table 2. Minimum required filter order for various cut-off frequencies

γ	f_{con}	f_{sbn}	FIR	Butterworth	Chebyshev	Inverse Chebyshev	Caeur
4	1/2	4/5	12	7	5	5	4
6	1/3	19/30	12	8	6	6	4
8	1/4	11/20	12	8	5	5	4
10	1/5	1/2	12	7	5	5	4
12	1/6	7/151	12	7	5	5	4
14	1/7	31/70	12	6	5	5	4
16	1/8	17/40	12	6	5	5	4

6.1.2. The Filters Response

An ideal filter will have an amplitude response that is unity or at a fixed gain for the frequencies of interest in the passband and zero everywhere else that is in the stop band. The magnitude response of all considered filters was plotted in Figure 4 for various filter orders n. The cut-off frequency normalized by Nyquist frequency was arbitrary set to 0.8. For all filter types, it appears the higher the filter order, the closer the transfer function to the ideal low-pass filter but also the higher the spatial and temporal complexity. The impulse response also increases with increasing filter order; hence higher filter order implies greater band-limiting. Also, it appears unlike, the IIR filters, FIR filters require higher orders to approximate the ideal low-pass filter.

Now we consider a normalized cut-off frequency of 0.5. The frequency is converted to radians per second and attenuations are evaluated in decibels. For all filters, the same pass-band edge frequency, 1dB pass-band ripple and 60 dB stop band attenuation are considered. Filters orders are set to the minimum required values for the above settings as computed on Table 2. The comparison plot is shown in Fig. 5.

We can see the advantage with the Butterworth filter compared to other filters is it has a maximally flat magnitude response, with no passband ripple and a roll-off of -20dB per pole. The Butterworth scheme optimizes the flatness of the passband response at the expense of roll-off and a relatively wide transition region from passband to stop band, with average transient characteristics. This filter is a good compromise between attenuation and phase response.

The Chebyshev filter has a smaller transition region and a faster roll off than the same order Butterworth filter, at the expense of ripples in its pass band. The Chebyshev response appears to be an optimal tradeoff between the pass-band ripple and the roll-off. Chebyshev filters minimize the error between the ideal and the actual filter characteristic over the range of the filter, but with ripples in the passband. For all-pole filters, the Chebyshev filter gives the best amplitude discrimination, followed by the Butterworth.
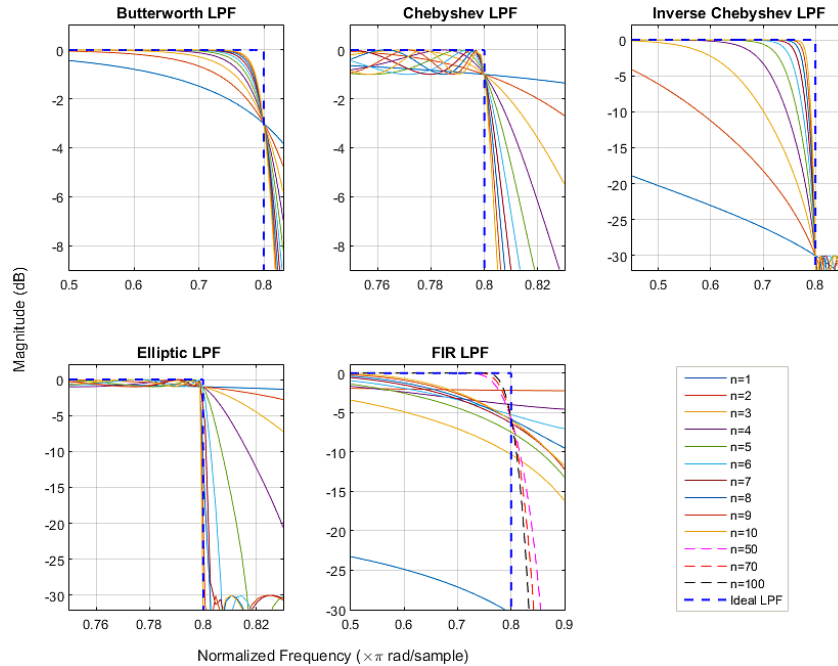
Figure 4. Magnitude response of various orders LPF filters against ideal filter's

Elliptic filters provide the fastest roll-off for a given order or number of poles, but their design is more complex. The amount of ripple in the stop-band will not be an issue, as long as the signal to be rejected is sufficiently attenuated. FIR filter is optimized to obtain better transient response due to a linear phase or constant delay in the passband and hence a poorer frequency response or less amplitude discrimination.
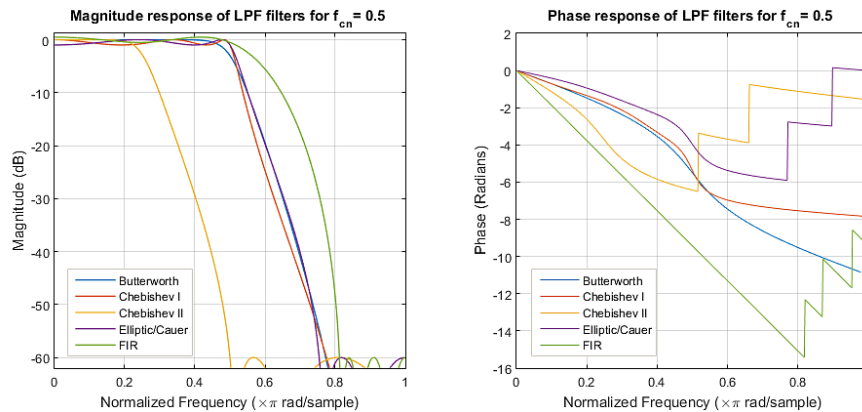

Figure 5. Magnitude and phase response of digital LPF filters

Just like the Butterworth filter, the Inverse Chebyshev filter has flat passband and wide transition band as well as good amplitude and transient behaviour. This filter has a steeper roll-off but a little more stopband ripple than Butterworth filters. It has ripple only in the stopband. The Chebyshev filters improve on the amplitude response at the expense of transient behaviour. The frequency input to the Inverse Chebyshev design function sets the beginning of the stopband rather than the end of the passband. That is why this filter appears to be the only one that assures the signal attenuation to be bigger than the stop band required attenuation at the cut-off frequency.

6.1.3. The Bhattacharyya Distance to Evaluate the Divergence between Simulated Shadowing and Theoretical Lognormal Distribution

We consider the results on the table above for $f_{con} = 1/i, \ i \in \{2,3,4,5,6,7,8\}$. The computed minimum filter orders are shown in Table 2 for all considered filters. The Bhattacharyya distance between distributions of the simulated shadowing from all considered low pass filters and the theoretical lognormal distribution is evaluated using a Monte Carlo method and comparison plots are shown in Fig. 6 and Fig. 7. They clearly show

the 5th-order inverse Chebyshev filter minimizes the divergence followed by the 7-th order Butterworth filter for all f_{con}. The largest distance is given by the FIR low pass filter. We can also see that the higher the cut-off frequency, the lower the divergence.

Similar results were obtained for other statistical distances like the Hellinger distance, the Earth-Mover's distance, the Cosine distance, the Kullback-Leibler and the Chebyshev distance.

Table 3. The Inverse Chebyshev filter has the minimum distance for all frequencies

BUTT	CHEB-1	CHEB-2	CAEUR	FIR	fcon
4.06	4.06	4.01	4.15	4.20	1/2
4.13	4.14	4.06	4.26	4.33	1/3
4.17	4.17	4.05	4.30	4.36	1/4
4.22	4.23	4.07	4.29	4.37	1/5
4.26	4.27	4.09	4.26	4.36	1/6
4.29	4.31	4.12	4.29	4.37	1/7
4.32	4.33	4.14	4.40	4.43	1/8
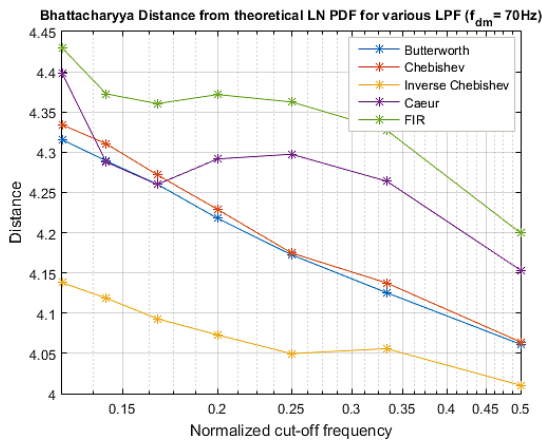
Figure 6. Divergence between simulated and theoretical shadowing using a Monte Carlo method
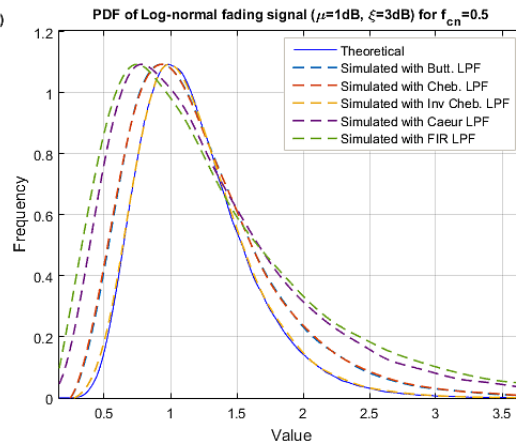
Figure 7. PDF of filters input and output

6.1.4. The Filters Implementation Cost

Matlab filter design tool was used to compute the hardware implementation cost of the different filters for all considered values of f_{con}. The target parameters were the filter order or the number of states (Ns), the number of adders (Na) and multipliers (Nm), and the number of adders and multipliers per input sample (Ms and As respectively). Results are available in Table 4and Fig. 8. They show that the elliptic filter is the least hardware resource consuming among all considered filters followed by the Inverse Chebyshev filter.The FIR filters require a large filter order and therefore a high computational cost to achieve desired specifications. IIR filters are stable, with smaller group delays and shorter transient response while their principal drawback is the phase non-linearity as can be seen on Fig. 5. However they are adequate to be used to optimize on computational resources in applications where linearity of phase is not a requirement.

Table 4. Filters implementation cost data (a and b)

f_{con}	1/2					1/3					1/4					1/5				
Filter	Bu	Ch1	Ch2	Ca	Fir	Bu	Ch1	Ch2	Ca	Fir	Bu	Ch1	Ch2	Ca	Fir	Bu	Ch1	Ch2	Ca	Fir
Nm	15	11	11	9	13	17	13	13	9	13	17	11	11	9	13	15	11	11	9	13
Na	14	10	10	8	12	16	12	12	8	12	16	10	10	8	12	14	10	10	8	12
Ns	7	5	5	4	12	8	6	6	4	12	8	5	5	4	12	7	5	5	4	12
Ms	15	11	11	9	13	17	13	13	9	13	17	11	11	9	13	15	11	11	9	13
As	14	10	10	8	12	16	12	12	8	12	16	10	10	8	12	14	10	10	8	12

a)

f_{con}	1/6					1/7					1/8				
Filter	Bu	Ch1	Ch2	Ca	Fir	Bu	Ch1	Ch2	Ca	Fir	Bu	Ch1	Ch2	Ca	Fir
Nm	15	11	11	9	13	13	11	11	9	13	13	11	11	9	13
Na	14	10	10	8	12	12	10	10	8	12	12	10	10	8	12
Ns	7	5	5	4	12	6	5	5	4	12	6	5	5	4	12
Ms	15	11	11	9	13	13	11	11	9	13	13	11	11	9	13
As	14	10	10	8	12	12	10	10	8	12	12	10	10	8	12

b)
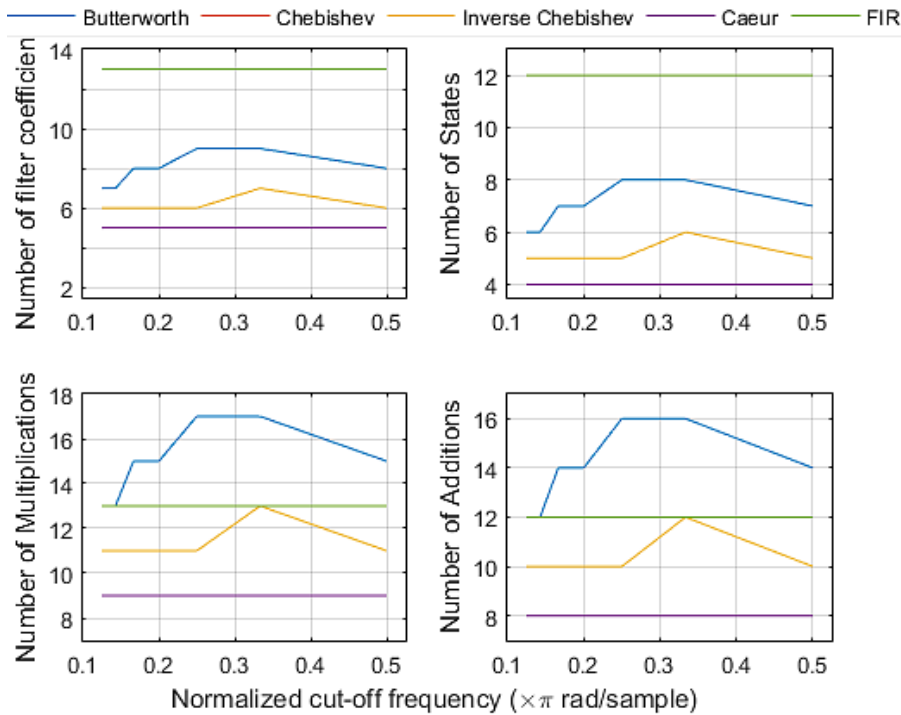
Figure 8. Implementation cost of considered filters

6.1.5. The Shadowing Outage Probability
The effect of co-channel interferers is neglected for simplicity. Thus we have $\mu_f \approx \mu$ and $\xi_f \approx \xi$. The shadowing standard deviation was set to 8dB as this value is commonly used in mobile networks link budgets and the impact of the sampling frequency was investigated. Fig 9 shows the lower the cut off frequency or higher the sampling rate, the more convergent are the outage probability curves with the best convergence around f_{cn}=1/8 (16 samples/Hz). The result appeared to be valid for all Doppler frequencies.

The shadowing standard deviation was then set to various values to simulate light (3dB), moderate (6dB and 8dB) and heavy shadowing (10dB) conditions. The Doppler frequency was set to 70Hz. Fig 10 shows that in highly noisy environment (SNR less than or equal to -3dB) and whatever the shadowing severity (Light, Moderate or Heavy), the shadowing model based on the Inverse Chebyshev LPF presents a better behavior compared to all other filters with the lowest outage probability and appears to be the best fit to the expected analytical curve. Around -3dB, all considered LPF presents similar performances whereas in better conditions with high SNR

environments the FIR filter-based model appears to be a better scheme even though the closest agreement to the expected curve is still given by the Inverse Chebyshev based model. The simulation was performed for other LTE channels using other Doppler frequencies (5Hz and 300Hz) and the result appeared to be invariant for all Doppler frequencies and for all filters sampling rates.
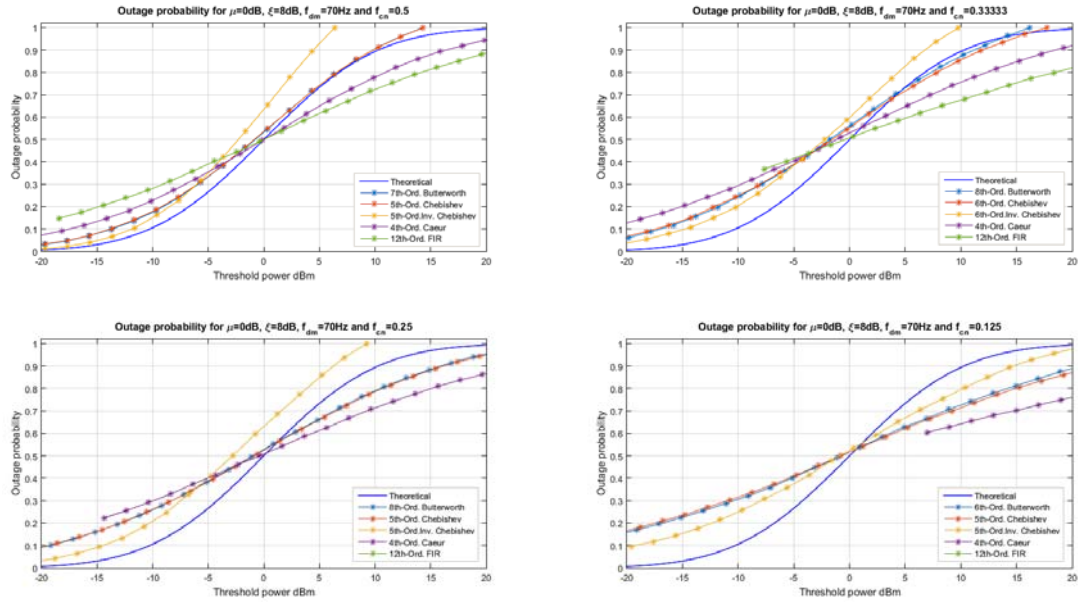

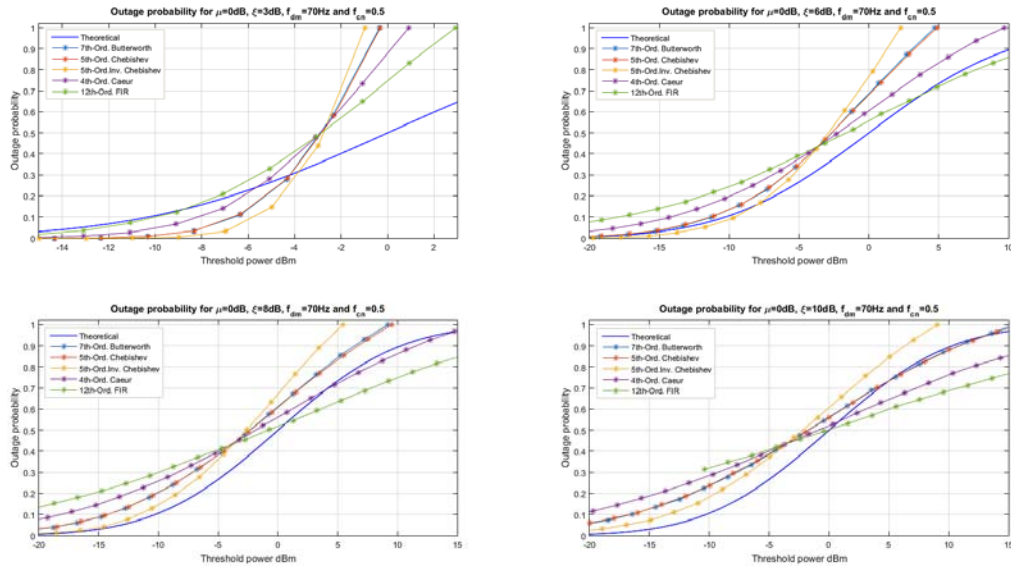**Figure 9**. Impact of LPF cut off frequency on shadowing outage probability

Figure 10. Impact of shadowing severity on the outage probability

6.1.6. The Shadowing spatial autocorrelation

Shadowing autocorrelation for μ=1dB, ξ=8dB, f_{dm}=70Hz and f_{cn}=0.5
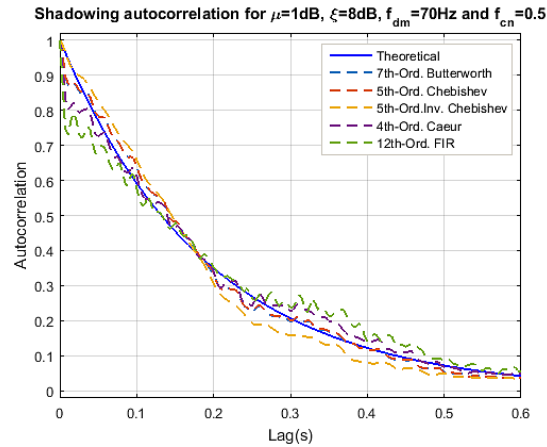
Figure 11. Shadowing autocorrelation for various low pass filters

All considered low pass filters show similar performance autocorrelation-wise as shown in Fig. 11. These performances are equal when the lag approaches 0.2s although for lags greater than 0.2s, we observe a faster decorrelation for Inverse Chebyshev filter. However, throughout all lag values from 0 to the decorrelation distance, Butterworth and Inverse Chebyshev filter show the closest agreement to the analytical curve

6.2. The Proposed Suzuki Fading Simulator

Multiplying correlated Rayleigh random variable with correlated lognormal random variable will produce a correlated Suzuki random variable. For simplicity, the Suzuki process generation will follow these steps.
1) Define the severity or depth of the slow fading by adjusting μ and ξ. Or define the environment EPA, EVA, ETU or HST.
2) Generate the lognormal fading using a 5th-order Inverse Chebyshev filter with the above parameters.
3) Generate correlated Rayleigh Random Variable using the Young's simulator.
4) Multiply the above Rayleigh and Lognormal variables to get the Suzuki fading sequence for the flat fading channel.

The general diagram of the proposed Suzuki fading simulator is shown below
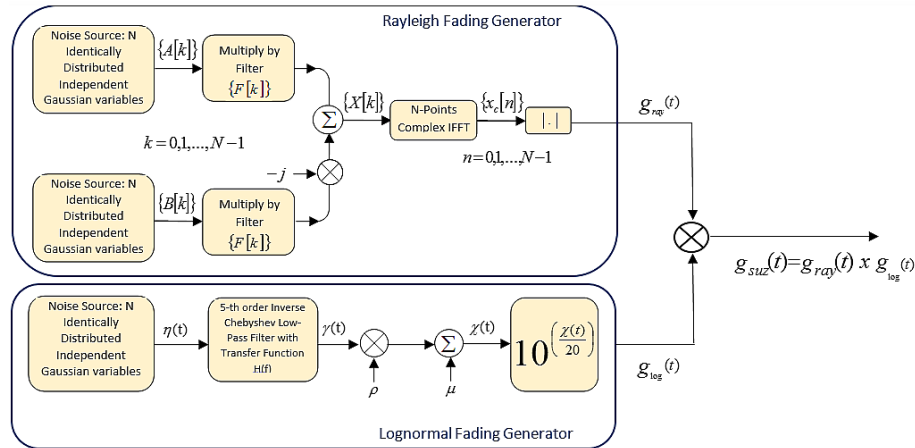
Figure 12. Proposed Suzuki fading simulator

6.3. Performances and Statistics
The performance of the proposed Suzuki fading simulator can then be evaluated through first and second order statistics of the fading.

6.3.1. The Generated Fading Signal
The generated fading sequences are presented in Fig. 13 and Fig. 14. We can notice lognormal fading component presents less fluctuations but deeper fades compared to fast fading component. The resulting Suzuki signal follows the slow fading component while being affected locally by the fast fading component. The resulting signal presents characteristics of both Rayleigh and lognormal signals.
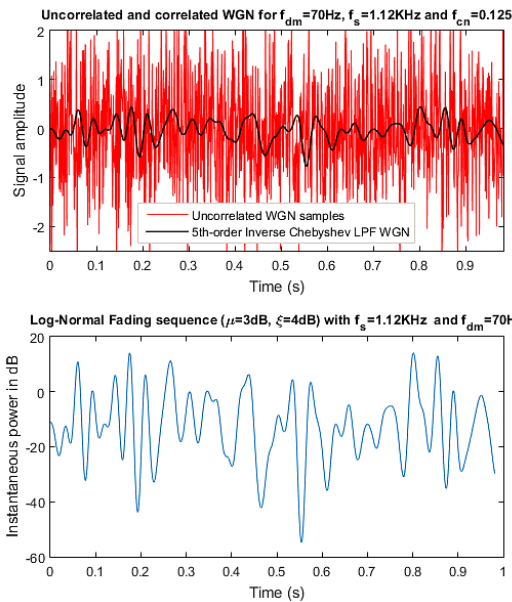
Figure 13. Uncorrelated and correlated WGN (top) and resulting lognormal fading sequence (bottom) for f_{dm}=70Hz
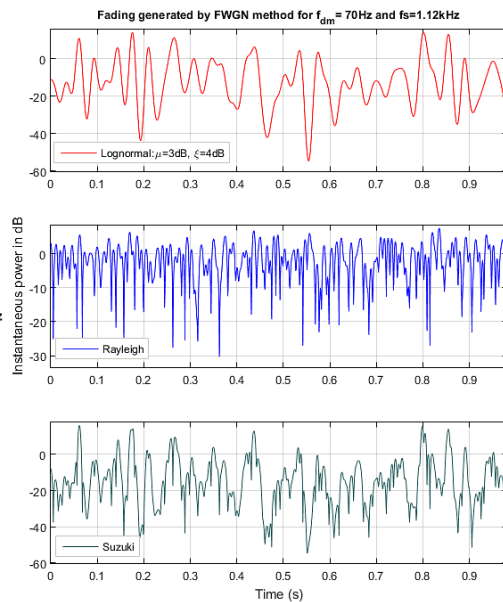
Figure 14. Lognormal, Rayleigh and Suzuki fading sequences for f_{dm}=70Hz

6.3.2. The Probability Density Function
Simulated PDF were plotted and the result is shown on Fig. 15 and Fig. 16. They are in agreement with theoretical expectations.
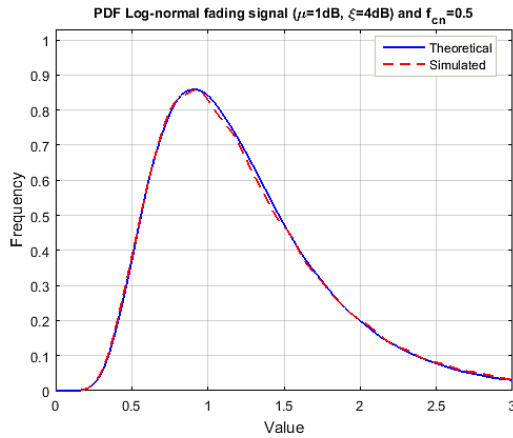
Figure 15. PDF of simulated shadowing using Inverse Chebyshev LPF output against theoretical Lognormal PDF
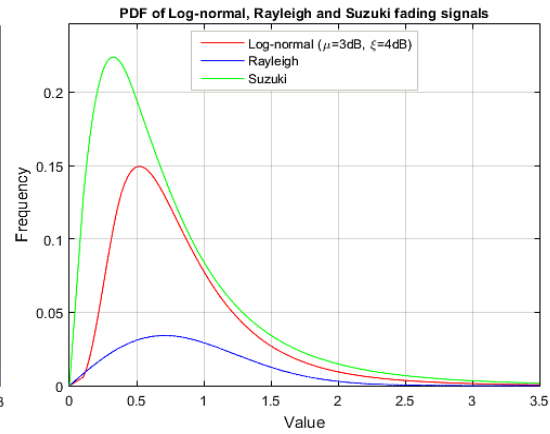
Figure 16. PDF of Suzuki signal against Lognormal and Rayleigh

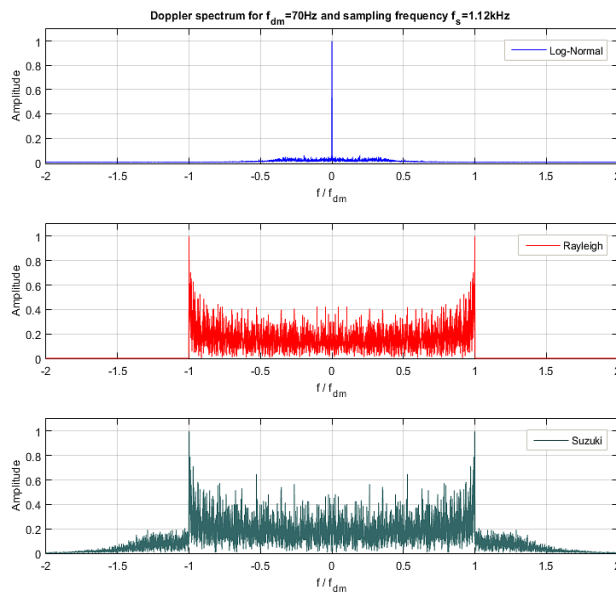### 6.3.3. The Doppler Spectrum

Figure 17. Simulated Lognormal, Rayleigh and Suzuki Doppler spectra

Simulated power spectra were plotted and the result is shown on Fig. 17. As for the PDF, they are in agreement with expected theoretical curves.
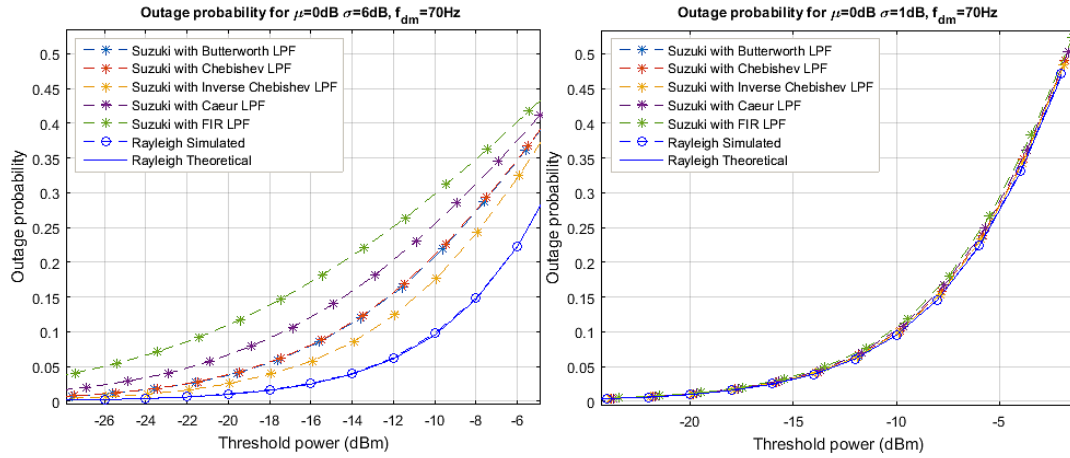
6.3.4. The Outage Probability

Figure 18. Effect of shadowing severity on outage probability for f_{dm} =70Hz

The outage probabilities for various thresholds and for the Suzuki fading using various LPF for the lognormal component, were evaluated, and compared to analytical values. The Inverse Chebyshev LPF allows a lower outage probability whereas the FIR LPF gives the highest. Moreover Fig.18 shows the outage probability of the simulated Suzuki fading for all considered LPF aligns with Rayleigh fading outage probability when the shadowing severity level becomes negligible ($\xi \to$ 0dB). In Fig. 19 and Fig. 20, the Inverse Chebyshev LPF remains the best trade-off for Suzuki fading outage probability. As one would expect from the results on shadowing, this performance parameter is minimized by the use of the Inverse Chebyshev LPF. This result happened to be valid for both LTE channels and for various levels of shadowing and for various Doppler frequencies. The illustrations below show the result for EPA, EVA and ETU channels in presence of light and moderate shadowing.
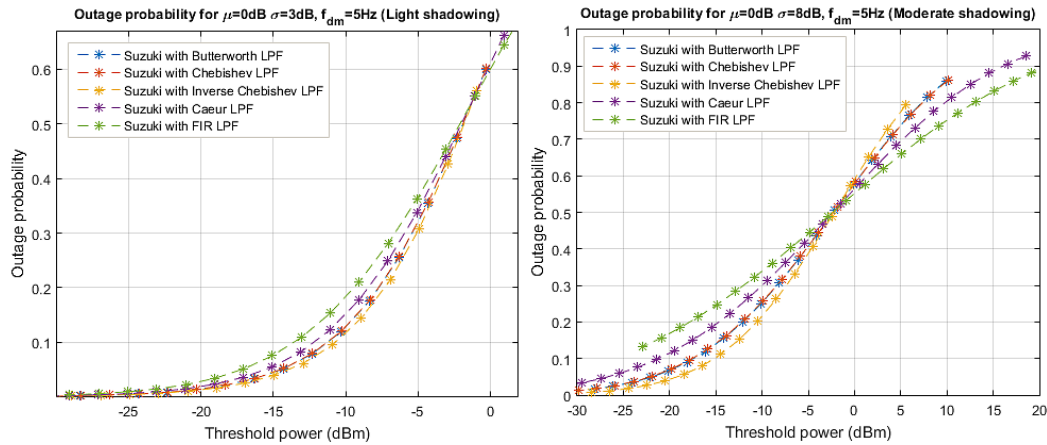

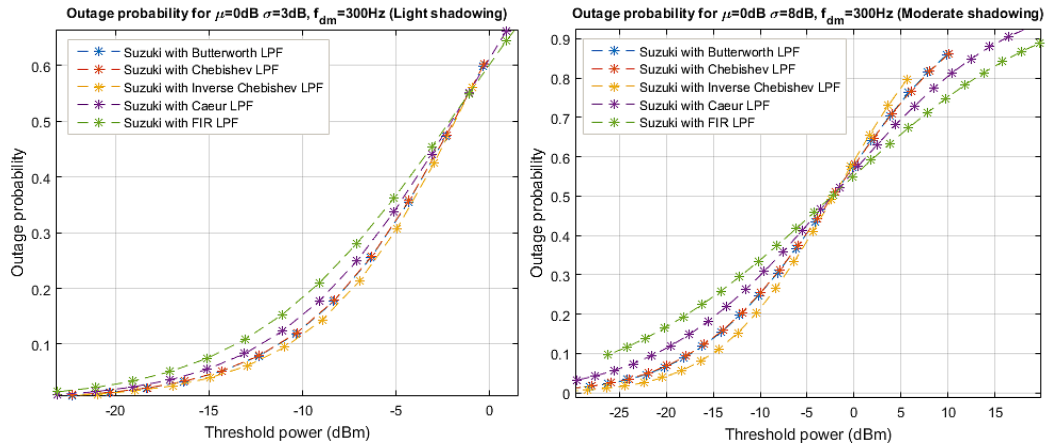**Figure 19**. Outage probability of Suzuki fading for f_{dm}=5Hz

Figure 20. Outage probability of Suzuki fading for f_{dm}=300Hz

VII.   Conclusion

In this paper, an efficient fading channel generator for Suzuki distribution with the lognormal shadowing component based on an IIR low pass filter is proposed. For the optimization of this component, the Butterworth, Chebyshev, Inverse Chebyshev and Cauer low pass IIR filters were evaluated as well as the FIR low pass filter based on Parks-McClellan method for a constrained optimal order and equiripple FIR filter. Discrimination criteria were the magnitude and phase responses, minimum required filter, filter hardware implementation cost, shadowing outage probability and autocorrelation, as well as the statistical divergence between the simulated and theoretical shadowing distributions. Above all, the 5-th order Inverse Chebyshev low pass filter happened to be the best trade-off for shadowing generation as it showed the closest agreement between the expected theoretical and the simulated results. Finally, output signal samples and various order statistics confirmed the effectiveness of the proposed Suzuki fading channel generator.

Acknowledgements

References

[1]   Vidhi Sharma, Dinesh Kumar Dhaka. **"**Review Paper on Second Order Statistics of Various Fading Channels". International Journal of Advanced Research in Electrical, Electronics and Instrumentation Engineering. Vol. 3, Issue 7, July 2014
[2]   Matthias Pätzold. "Mobile fading channels." Second Edition**.** John Wiley & Sons, Ltd. 2012. Chap. 6
[3]   Suzuki, H. "A Statistical Model for Urban Radio Propogation," in *IEEE Transactions on Communications*, Vol. 25, Issue 7, July 1977, pp. 673 - 680.
[4]   Fernando P. Fontan, Perfecto MariñoEspiñeira. "Modelling the Wireless Propagation Channel. A simulation approach with Matlab". John Wiley & Sons Ltd, Sept. 2008
[5]   N.M.A.E.D. Wirastuti, N.P. Sastra. "Application of the Suzuki distribution to Simulation of Shadowing Effects in Mobile Communication" 4th International Conference Information & Communication Technology and System ICTS 2008. PP 535-541
[6]   A. Krantzik and D. Wolf, "Distribution of the fading-intervals of modified Suzuki processes," in *Signal Processing V: Theories and Applications*. Torres, E. Masgrau, and M. A. Lagunas, Eds., Amsterdam, The Netherlands: Elsevier Science Publishers, B.V, 1990, pp. 361–364
[7]   Michel Mfeze, Emmanuel Tonye. "Comparative Approach of Doppler Spectra for Fading Channel Modelling by the Filtered White Gaussian Noise Method". *I*nternational *J*ournal of *C*omputer *S*cience and *T*elecommunications, Volume 6, Issue 11, December 2015.
[8]   Ricardo A. Losada. "Digital Filters with MATLAB". The MathWorks, Inc.May 18, 2008.
[9]   David J. Young and Norman C. Beaulieu, " The generation of correlated Rayleigh random variates by inverse discrete Fourier transform," IEEE transactions on Communications, vol. 48, pp. 1114-1127, July 2000.
[10]   M. C. Jeruchim, P. Balaban, and K. S. Shanmugan, "Simulation of Communications Systems", 2nd ed., New York: Kluwer Academic/Plenum Publishers, 2000.
[11]   Shashank Satyanarayana, Daniele Borio and Gérard Lachapelle "A Composite Model for Indoor GNSS Signals- Characterization, Experimental Validation and Simulation". Navigation, Volume 59, Issue 2, 2012
[12]   John Stensby. "The Butterworth Low-Pass Filter". October 2005. www.ece.uah.edu/courses/ee426/Butterworth.pdf
[13]   John Stensby. "Chebyshev Filters." EE648, August 2011
[14]   Kerry Lacanette. "A Basic Introduction to Filters—Active, Passive, and Switched-Capacitor" National Semiconductor Application Note 779 April 21, 2010
[15]   Sophocles J. Orfanidis. « Lecture Notes on EllipticFilter Design". Rutgers University. November 20, 2006.
[16]   Miroslav D. Lutovac, Dejan V. Tosic. "Elliptic Rational Functions". The Mathematica Journal; Wolfram Media, Inc, 2005
[17]   Rabiner, Lawrence R., and Otto Herrmann. "The Predictability of Certain Optimum Finite-Impulse-Response Digital Filters." IEEE®Transactions on Circuit Theory. Vol. 20, Number 4, 1973, pp. 401–408
[18]   Sung-Hyuk Cha "Comprehensive Survey on Distance/Similarity Measures between Probability Density Functions". International Journal of Mathematical Models and Methods in Applied Sciences Issue 4, Volume 1, 2007

[19]   Dorra Ben CheikhBattikh. "Outage probability formulas for cellular networks : contributions for MIMO", CoMP and time reversal features. Other. Telecom ParisTech, 2012. Ch2, 4, 6, 7

[20]   Fabien H´eliot, Xiaoli Chu, Reza Hoshyar, Rahim Tafazolli. A Tight Closed-Form Approximation of the Log-Normal Fading Channel Capacity. IEEE Transactions on Wireless Communications. Vol. 8, No. 6, June 2009

[21]   P. Mohana Shankar. "Fading and Shadowing in Wireless Systems" Springer Science & Business Media, 7 Dec 2011, Chap 4.

[22]   Marceau Coupechoux. «Link Budget 4G». NFRES/RMS. Telecom ParisTech. March 2007.

[23]   Andreas F. Molisch. "Wireless Communications" Second Edition. John Wiley & Sons Ltd, Sept. 2011. Chap.5, 8

[24]   Mohamed Ibnkahla. "Signal processing for mobile communications handbook". CRC Press LLC 2005. Chap 5

[25]   http://morse.colorado.edu/~tlen5510/text/classwebch4.html#x27-810004.1.1

[26]   Klaus Wehrle, Mesut Günes, James Gross. "Modeling and Tools for Network Simulation". Springer Science & Business Media, Sep 22, 2010

[27]   http://www.teletopix.org/4g-lte/slow-fading-margin-in-lte-with-example-of-standard-deviations-in-slow-fading/

[28]   William H. Tranter, K. Sam Shanmugan, Theodore S. Rappaport, Kurt L. Kosbar. "Principles of Communication Systems Simulation with Wireless Applications".PRENTICE HALL. Professional Technical Reference. Upper Saddle River, New Jersey. 2004 Chap 14

[29]   M. Gudmundson, "Correlation model for shadow fading in mobile radio systems," in *Electronics Letters*, vol. 27, no. 23, pp. 2145-2146, 7 Nov. 1991.

[30]   Andrea Goldsmith. "Wireless Communications" Stanford University. 2004. 427 Pages Chap 2

[31]   Jean-Marc Kelif1, Marceau Coupechoux "Joint Impact of Pathloss Shadowing and Fast Fading - An Outage Formula for Wireless Networks". Institut TELECOM, TELECOM ParisTech and Orange Labs. January 12, 2010

[32]   C. Fischione, M. D'Angelo "An Approximation of the Outage Probability in Rayleigh-lognormal Fading Scenarios"University of California at Berkeley. 2008

[33]   KavehPahlavan, Allen H. Levesque "Wireless Information Networks". John Wiley & Sons, 7 nov. 2005 - 760 pages, Chap.4.

[34]   Aleksandra M. Mitic and Mihajlo C. Stefanovic "Second Order Statistics of the Signal in Ricean-Lognormal Fading Channel with Selection Combining". SER.: ELEC. ENERG. vol. 20, no. 2, August 2007, 163-173